J Mater Sci (2020) 55:14953–14964

Energy materials

Synthesis of nanostructured TiC/TiO_2 with controllable morphology on carbon fibers as photocatalyst for degrading RhB and reducing Cr(VI) under visible light

Bo Lv[1], Lihong Xia[1], Yu Yang[1], Xiaoming Wang[1], Chen Yin[1], Yaoping Li[1], and Fuqin Zhang[1,*]

[1] *National Key Laboratory of Science and Technology on High-Strength Structural Materials, Central South University, Changsha 410083, China*

Received: 22 February 2020
Accepted: 10 July 2020
Published online: 20 July 2020

ABSTRACT

Carbon fibers (CFs) and TiH_2 were used as raw materials to grow TiC on the surface of CFs in a molten salt system. After hydrothermal reaction with sodium hydroxide, part of TiC was converted into sodium titanate. The sodium ions were substituted by H^+ by the hydrochloric acid solution treatment. CFs@TiC/TiO_2 composite was generated after high-temperature treatment. XRD, Raman, XPS, SEM, and AFM were used to characterize the structure and morphology of the composites. Results showed that a porous TiC film layer was homogeneously formed which was evenly wrapped on the surface of CFs. Through hydrothermal, displacement, and calcination processes, part of TiC was transformed into anatase TiO_2 with controllable morphology. Photocatalytic degradation experiments by the composite catalysts were carried out. The chemical reactions involved in the formation of composite structures and their effects on photocatalysis were analyzed and discussed. Notably, the morphology characteristics of the heterogeneous structure has a marked impact on the photocatalytic degradation of organic pollutants and photocatalytic reduction of hexavalent chromium [Cr(VI)]. Furthermore, the composites can be easily recycled and reused with good reactivity.

Introduction

The discharge of industrial sewage and organic wastewater pollutes the environment and threatens the health of wildlife and human [1, 2]. The development of society and the energy crisis has increased the demand for clean energy [3–5]. Photocatalysis is an excellent solution for sewage treatment and environmental protection [6–8].

Address correspondence to E-mail: zhangfqtx@163.com

https://doi.org/10.1007/s10853-020-05071-x

The application of TiO_2 as a photocatalyst has attracted significant attention due to its fast, non-selective, and complete degradation of organics with respect to biodegradation technique. Meanwhile, TiO_2 is also superior to the traditional chemical oxidation methods due to its high photocatalytic activity, low cost, and non-toxicity [9–12]. Therefore, TiO_2 has broad application prospects in environmental pollution control. The catalytic activity of TiO_2 is often closely related to its microscopic morphology. The research on TiO_2 at the micro- or nanometer scale has attracted extensive attention. One of the technical difficulties of using TiO_2 nanopowders in water or air treatments is the recovery and reuse of TiO_2, which normally bears a very high cost. TiO_2 powder particles can also become agglomerated in water, which reduces their specific surface area and greatly reduces the density of the reactive sites [13]. Therefore, researchers have attempted to immobilize TiO_2 nanomaterials on other solid substrates, such as SiO_2 [14–16], Al_2O_3 [17, 18], activated carbon [19, 20], and carbon fibers [21, 22]. Compared with other basic materials, CFs have unique properties, including good flexibility, excellent mechanical strength, and acid and alkali corrosion resistance [23–25].

Nano-TiO_2 can be introduced to the surface of CFs through various methods, such as chemical vapor deposition, surface spraying, sol–gel, and supercritical synthesis [26–31]. These methods are complex and require specialized equipment. In this work, TiO_2 nanomaterials were generated on the surface of CFs through the TiC intermediates. TiC was converted to titanate nanowires through a hydrothermal reaction and an ion exchange process. The titanate was converted into TiO_2 after calcination. The process is simple, easy to control. TiO_2 was successfully fixed on CFs.

In recent years, TiC has been found to have the electronic structure and the catalytic activity similar to platinum [32]. The anisotropic structures of nanomaterials can provide favorable carrier transport channels and have therefore attracted the attention of photoelectric catalysis through semiconductors [33, 34]. The TiC transition layer, formed on the surface of CFs, offers a strong substrate for TiO_2 grown on CFs. The uniformly distributed TiO_2 can effectively prevent the shedding of the TiO_2 thin film and minimize the agglomeration of nanoparticles. Thus, its catalytic performance can be effectively optimized and maintained. TiC, which is a transition metal carbide, shows similar chemical stability and catalytic performance to precious metals. After hydrothermal reaction with NaOH, sodium titanate nanowires with controllable micromorphology were obtained on the surface of CFs. After ion exchange and calcination, CFs@TiC/TiO_2 composite materials were obtained. The photocatalytic degradation of RhB dye and reduction of Cr(VI) was studied, and the influence of different morphology of the heterogeneous structure of CFs@TiC/TiO_2 on the degradation of RhB and reduction of Cr(VI) were discussed.

Experimental

Preparation of CFs@TiC samples

The synthesis procedure is illustrated in Fig. 1. CFs (Japan T700, approximately 7 μm in diameter) were used as a carbon source, and TiH_2 powder (Shanghai Aladdin Reagent Co., Ltd., 200 mesh) was used as Ti raw material. The CFs were resin-coated, and it is necessary to purify the CFs. The resin-coated CF fiber bundle was placed into the Soxhlet extractor, and the resin on the fiber surface was removed by reflux with acetone at 80 °C for 72 h. The dispersed pure fibers were collected and vacuum-dried for 24 h at 105 °C. TiH_2 particles and KCl (analytical pure) were fully mixed before the CFs were dispersed in the mixture in an alumina crucible. The molar ratio of Ti/C was 0.5, and the mass of KCl was 10 times the weight of the total reactants. The alumina crucible was placed in a tube furnace purged with argon as a protective gas. The temperature was programmed to rise at a rate of 10 °C/min until 1000 °C and hold for 3 h. The sample was cooled to room temperature and thoroughly washed with boiling distilled water several times to remove the excess salt. The fibers were vacuum-dried for 24 h.

Synthesis of CFs@TiC/TiO_2 composite materials

The 0.1 g of TiC-modified CFs and 20 mL of 1 mol/L sodium hydroxide solution were placed in a 25-mL PL high-pressure hydrothermal reactor. The heating rate was 3 °C/min, and the reaction temperature was 240 °C, held for different durations (2 h, 4 h, 6 h, 10 h). After the reaction, the sample was cooled down to room temperature at a controlled cooling rate of

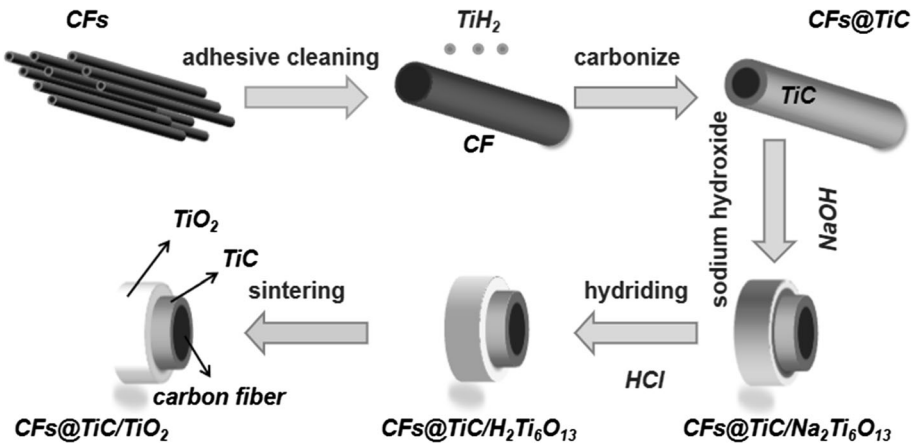

Figure 1 Schematic diagram of the material synthesis preparation process.

5 °C/min. The fibers were washed repeatedly with distilled water until the pH became neutral. Then, the fibers were placed into a beaker containing 10 mL of 1 moL/L hydrochloric acid solution. The fibers were soaked for 1 h at room temperature followed by washing until neutral. Finally, the fibers were placed into a crucible in a muff furnace. The temperature was raised to 400 °C at a rate of 5 °C/min, holding for 3 h before being cooled and collected.

Structural and morphological characterization

An X-ray diffractometer (D/max2550pc, PIGAKV Co., Ltd.) with a copper target and a scanning step of 0.02° was used to analyze and detect the material crystal structure. The phase structure of the fibers was analyzed using a microlaser Raman spectrometer (LabRAM HR800). The chemical composition and element binding energies were analyzed by XPS (k-alpha, Thermo Fisher Scientific). An electron scanning electron microscope (Helios Nanolab G3 UC, FEI) was used to observe the surface microstructure of the fibers. A scanning probe microscope (NanoManVS + Multimode, Veeco) was used to observe the 3D morphology of the sample surface at the nanoscale. A xenon lamp (PLS-SXE300, Perfect Light, wavelength > 400 nm, UV filter: UVCUT400) was adopted as the light source for photocatalytic reactions. The load of the photocatalysts was 50 mg in a 50 mL solution. The concentration of the RhB solution was 20 mg/L, and the concentration of Cr(VI) solution was 10 mg/L. In total, 0.1 mL of citric acid (concentration of 100 g/L) was added as the trapping agent. The concentration of Cr(VI) was measured by the diphenylcarbazide spectrophotometry method. To eliminate the adsorption effects, the sample solution was stirred in the dark for 30 min before the measuring of the photodegradation rate under the light.

Results and discussion

Structural characteristics

At present, considerable research focuses on obtaining a uniform and compact TiC film layer on the surface of CFs. Such films protect CFs or improve their surface properties to achieve their superior performance in composite materials, especially in enhancing their mechanical properties. In this work, we carefully choose TiC as the transition layer, which could bridge the catalyst and CFs and provide Ti raw material for TiO_2. It also offers a large active surface area. In the process of TiC synthesis, the bidirectional diffusion of C and Ti was most likely to cause the formation of a porous or uneven TiC film structure. Existing work [35] has shown that a layer of fragmented graphite structure exists on the surface of CFs, which helps the diffusion of atoms and can provide possibilities for surface reactions.

TiH_2 is decomposed into H and Ti raw materials at 400 °C. At 1000 °C, the Ti atoms continue to move toward CFs within the molten salt liquid phase and to form the TiC film layer on the CFs surface. Figure 2a shows the XRD spectra of the composite materials at different stages. The XRD showed peaks of 2θ angles at 35.9°, 41.7°, 62.4°, 72.3°, and 76.14°, which are formed on the surface of CFs. These peaks are associated with the crystal planes of (111), (200), (220), (311), and (222) of the typical cubic structure of

a TiC crystal, shown in the red curve in Fig. 2a. The formation of TiC hinders the X-ray penetration, and the intensity of amorphous CFs diffraction peak was reduced. The formed TiC film was then subject to the hydrothermal reaction, acid treatment, and calcination. Part of the TiC in CFs@TiC was transformed into anatase TiO_2 (named as CFs@TiC/TiO_2) composite material, identified by the anatase TiO_2 diffraction peaks of (101) and (200) at 25.3° and 48.0° [36] (blue curve in Fig. 2a), respectively.

Figure 2b shows the corresponding Raman spectra of samples at different stages. The Raman peaks without hydrochloric acid treatment mainly include four strong peaks at 275, 443, 700, and 915 cm^{-1} and three weak peaks at 192, 384, and 823 cm^{-1}. The Raman peak located at 275 cm^{-1} belongs to the Ti–O telescopic vibration, which involves two-coordinate O and is the characteristic vibration peak of titanate. The Raman peak located near 443 cm^{-1} belongs to the Ti–O bending vibration involving the tri-coordinate O. The Raman peak at 700 cm^{-1} is associated with the bending vibration of Ti–O in two-coordinate O. The Raman peak located near 915 cm^{-1} involves the stretching of Ti–O atoms, some of which coordinate with sodium ions to form Ti–O–Na^+. After hydrochloric acid treatment, the vibration peak of Ti–O–Na^+ at 915 cm^{-1} disappears due to the proton exchange. After heat treatment, the strong absorption peak of anatase TiO_2 (192 cm^{-1}) was observed, and the other existing peaks exhibited a blue shift.

XPS analysis

The electronic structure of the material surface and the chemical state of elements were analyzed and studied by XPS. The relevant chemical elements, such as Ti, O, and C, were monitored in the entire reaction process, shown in Fig. 3.

The XPS high-resolution scan of O 1*s* for CFs@TiC/TiO_2 is decomposed into three peaks at 530.0, 531.6, and 532.4 eV, which are attributed to the lattice O of anatase TiO_2, C–O, and the O atom near the oxygen vacancy. Two chemical states of O1*s* for pure anatase TiO_2 at 529.3 eV and 530.4 eV can be found, corresponding to Ti–O and hydroxyl group, respectively. The Ti–O binding energy was increased by 0.7 eV, attributed to the C-doping in CFs@TiC/TiO_2. The XPS spectrum of Ti 2*p* shows two major peaks with binding energies of 458.5 eV (2*p* 3/2) and 464.2 eV (2*p* 1/2). The difference in binding energy with an approximate separation of 5.7 eV between Ti2*p* ½ and Ti2*p* 3/2 is in good agreement with the standard binding energy value [37]. Compared to pure anatase TiO_2 (458.1 eV and 463.8 eV), the binding energies for both peaks were increased by 0.4 eV. This is because of the existence of the positively charged carbon in CFs@TiC/TiO_2, which may push the Ti atom toward the adjacent oxygen atom in the TiO_2 crystal. This will shorten the Ti–O bond and increase the binding energy of Ti2*p*. The small peak at 461.3 eV belongs to the Ti^{3+} oxidation state, which is associated with O vacancy or defect in the sample. From C 1*s* for CFs@TiC/TiO_2, the C bond peaks of C=O, C–O, and C–C sp^2 substrates are identified at 288.4 eV, 286.7 eV, and 284.8 eV. The peak at 281.6 eV is attributed to the binding energy of C-Ti. Compared to the sample of CFs@TiC, this peak disappeared mainly due to the conversion of TiC into TiO_2. From the co-existence of these chemical bonds, it is expected that some interstitial carbon in the TiO_2 lattice could form the Ti–O–C, which helps to promote the absorption in the visible light region and the charge carrier transfer required for photoexcitation. Carbon

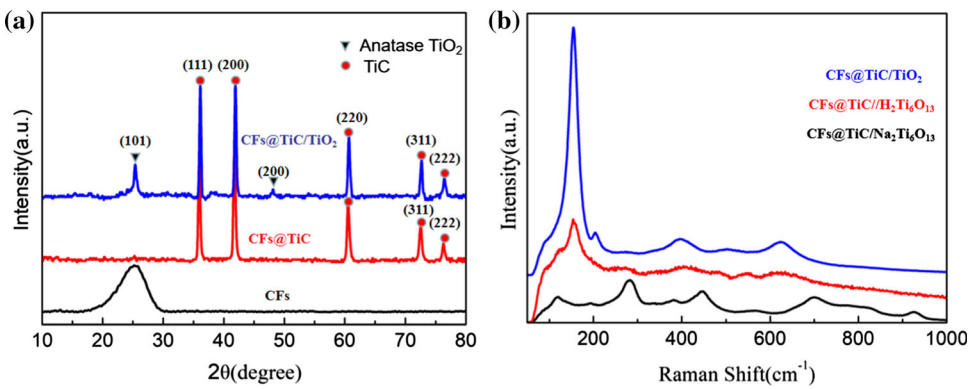

Figure 2 **a** XRD of CFs,CFs@TiC,CFs@TiC/TiO_2 and **b** Raman analysis of the CFs@TiC/$Na_2Ti_6O_{13}$, CFs@TiC/$H_2Ti_6O_{13}$, CFs@TiC/TiO_2.

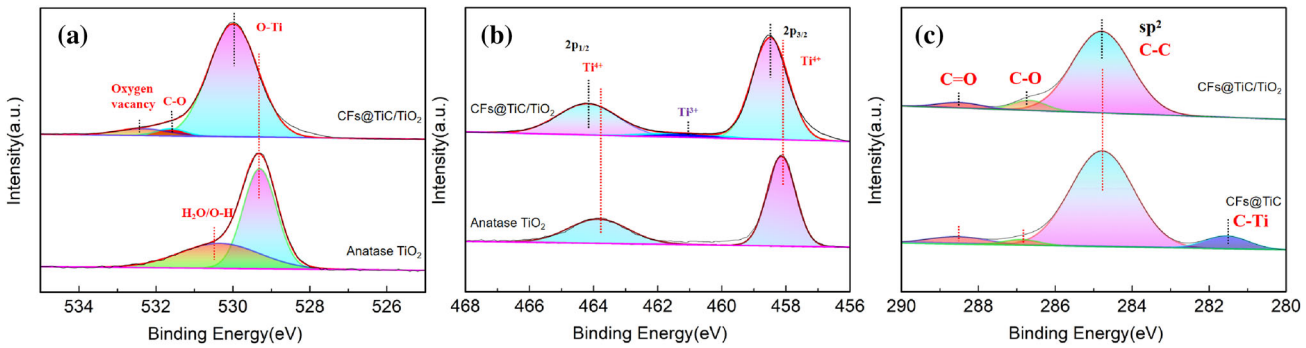

Figure 3 X-ray photoelectron spectroscopy analysis high-resolution scan of **a** O 1*s* and **b** Ti 2*p* of CFs@TiC/TiO_2 and Anatase TiO_2, and **c** C 1*s* of CFs@TiC/TiO_2 and CFs@TiC, respectively.

doping can improve the visible light absorption efficiency which in turn improves the photocatalytic performance.

SEM/AFM analysis

The morphology, size, location, and stability of active components of the catalyst have a close relationship and great influence on its catalytic activity [38, 39]. The growth process of sodium titanate nanowires on CFs was observed by SEM (Fig. 4). The effect of reaction time on the microstructure was studied.

After the molten salt reaction, the TiC was treated with NaOH basic solution in a hydrothermal reactor. On the surface of TiC, thin lamellar $Na_2Ti_6O_{13}$ was formed which is wedged into the fiber surface. This suggests that the growth of $Na_2Ti_6O_{13}$ at the interface junction between $Na_2Ti_6O_{13}$ and TiC is faster than on the $Na_2Ti_6O_{13}$ surface. The lamellar structure grows and thickens after the reaction time was 4 h or longer. At the reaction time of 6 h, the bottom of the lamellar structure cross-linked with contraction presents a floral structure. Once the reaction time was extended to 10 h, the neighboring $Na_2Ti_6O_{13}$ crystals interact to form a networked structure. Nanowires are also connected between the fibers.

Based on the observed morphological evolution, the growth process of sodium titanate in the hydrothermal reaction is proposed as follows. Small sodium titanate crystal seeds were first formed on the surface of the CFs. As the reaction progresses, the sodium titanate sheet grew and thickened. The nanowires at the bottom became close together, grew into each other, and acted as pestles similar to flowers. The other lamellar structures acted as petals and presented a floral structure. After the reaction time is prolonged, the petals on the surface grew together to form a network-like structure. Hence, the microstructures of the reaction products can be effectively controlled by simply controlling the reaction time. Active sites are concentrated in angles. To obtain the most catalytic active sites, the reaction time is determined to be 4 h.

SEM and AFM were both used to characterize the morphology of the fibers after each step of the reaction.

TiH_2 decomposes into Ti and H_2 at high temperatures. The presence of the KCl molten salt helps the distribution and reaction of Ti in the reaction system as it provides the liquid system needed for the reaction. This condition lowers the reaction energy barrier and reaction temperature between Ti and CFs. The C atoms were diffused outwardly, whereas the Ti atoms were moving toward the surface of CFs. The two-way diffusion of C and Ti forms a porous TiC structure on the surface of the CFs, as shown in Fig. 5d. The effective diameter of a single fiber increases from the original 7–9 μm, which proves the porous nature of the TiC with reduced packing density directly observed from the SEM images. Such a sponge-like structure provides a large number of reactive sites for the conversion of TiC to sodium titanate nanowires in the next reaction, as shown in Fig. 5g. The appearance of the porous structure provides a useful substrate for developing nanocatalysts.

The cross-sectional view of SEM images of the CFs, CFs@TiC, and CFs@TiC/TiO_2 is inserted in Fig. 5a, d, g, and j. The thicknesses of the TiC layer, $Na_2Ti_6O_{13}$ layer, and TiO_2 layer on CFs surfaces can be measured directly as 2.3, 0.60, and 0.35 μm, respectively.

The surface structure of a catalyst is an important affecting factor of its performance. The changes in the

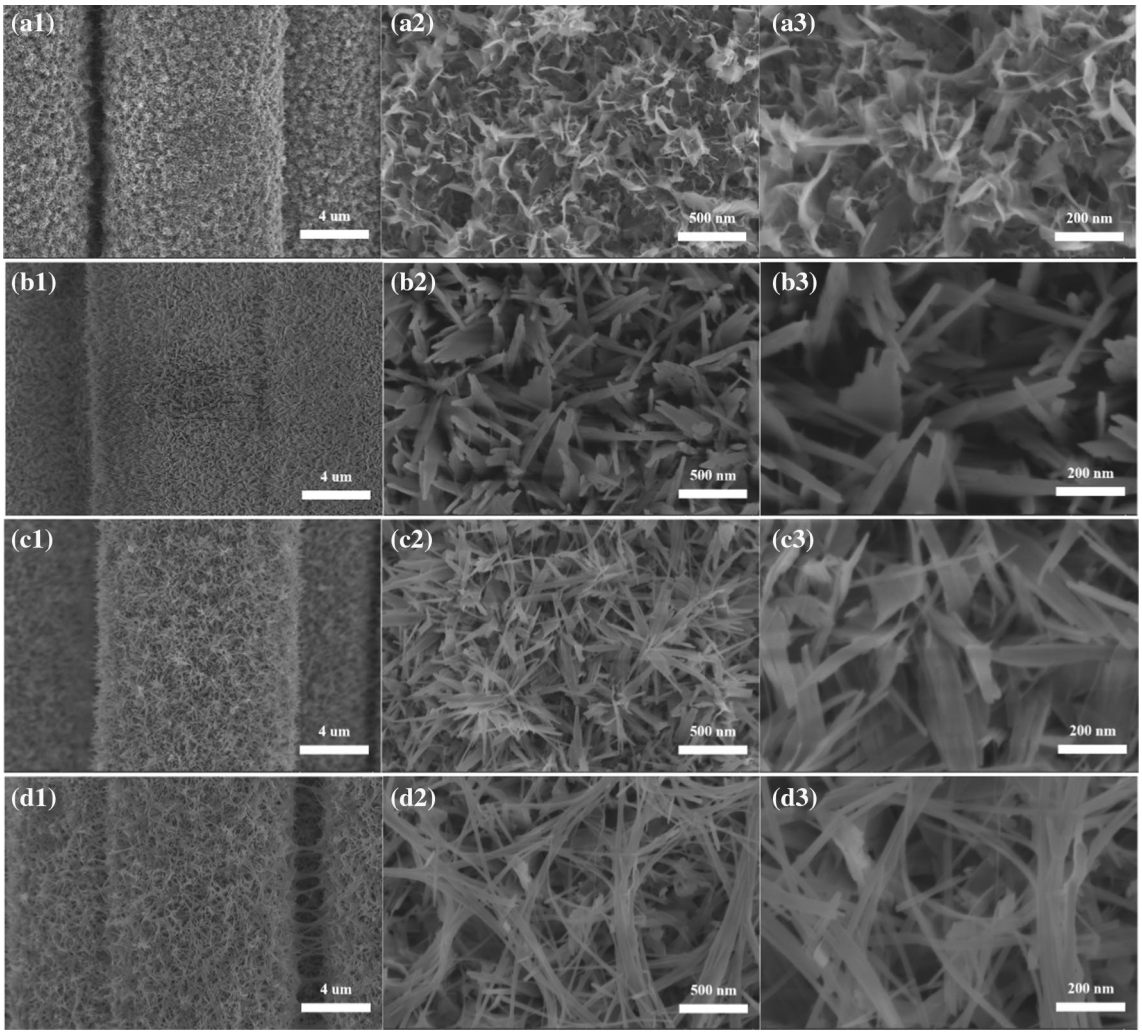

Figure 4 SEM images (at different magnifications) of samples prepared with different reaction times in hydrothermal reaction (**a** 2 h, **b** 4 h, **c** 6 h, **d** 10 h).

surface structure of the fibers during the entire reaction process can also be observed from the atomic force microscope. Figure 5b, e, h, and k reveals such changes. As shown in Fig. 5b, uneven grooves are present on the surface of CFs. This condition is conducive to the growth of TiC. Once the TiC was formed, the uneven granular structure can be observed on the surface of CFs, shown in Fig. 5e. As such, the interface area between TiC and CFs increases. Such a structure is favorable for the growth and support of TiO_2. Acicular sodium titanate nanowires were grown on the surface of the CFs by hydrothermal reaction with NaOH. Proton exchange and heat treatment converted the sodium titanate to the TiO_2 forming a multilayer heterogeneous nanostructure on CFs surface, which preserved the TiC nanostructures and maintained a high density of surface catalytic center.

Photocatalytic decomposition of RhB and reduction of Cr(VI)

The photocatalytic degradation of RhB and Cr(VI) solutions at room temperature under the visible light (wavelength > 400 nm) was studied to evaluate the photocatalytic activity of the prepared photocatalysts, including CFs, CFs@TiC, and CFs@TiC/TiO_2. Repetitive experiments were also carried out to test the reusability of the catalysts. The experimental results are shown in Fig. 6a–d.

Before catalytic degradation, the tested aqueous solution was stirred in the dark for 30 min to achieve adsorption equilibrium. Neither CFs nor CFs@TiC

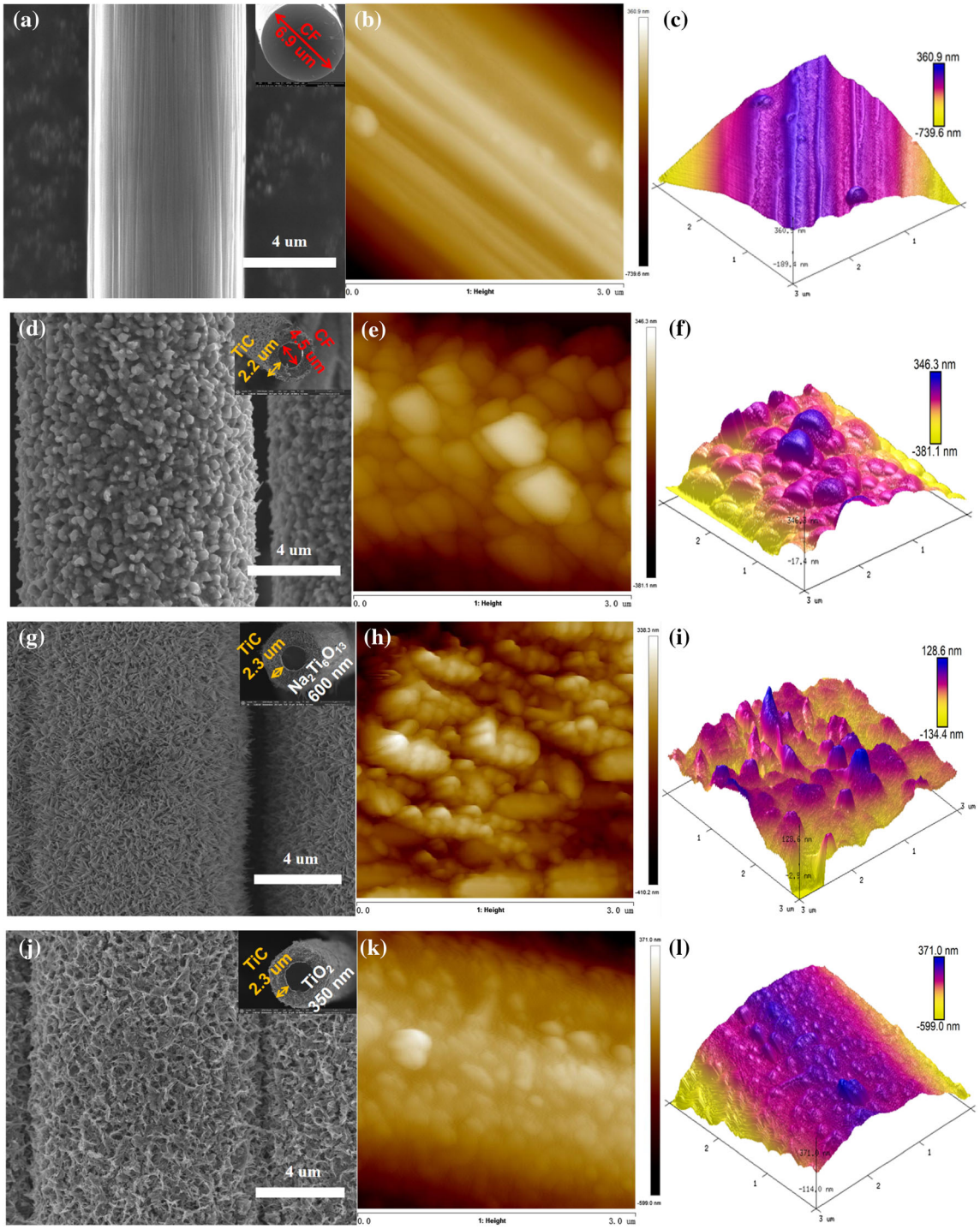

Figure 5 SEM and AFM images of **a**–**c** CFs, **d**–**f** CFs@TiC, **g**–**i** CFs@TiC/$Na_2Ti_6O_{13}$ (4 h), **j**–**l** CFs@TiC/TiO_2 (4 h).

degrades RhB and reduces Cr(VI) significantly. After partial TiC is converted into TiO_2, a heterogeneous structure of TiC and TiO_2 was formed on the surface of CFs, which greatly increases the degradation rate of RhB and the reduction rate of Cr(VI). The CFs@TiC/TiO_2 was used repeatedly for three times. The results show that the degradation rate and efficiency were maintained constant. Therefore, TiO_2, supported by CFs, can be reused under our experimental conditions with good chemical and physical stabilities.

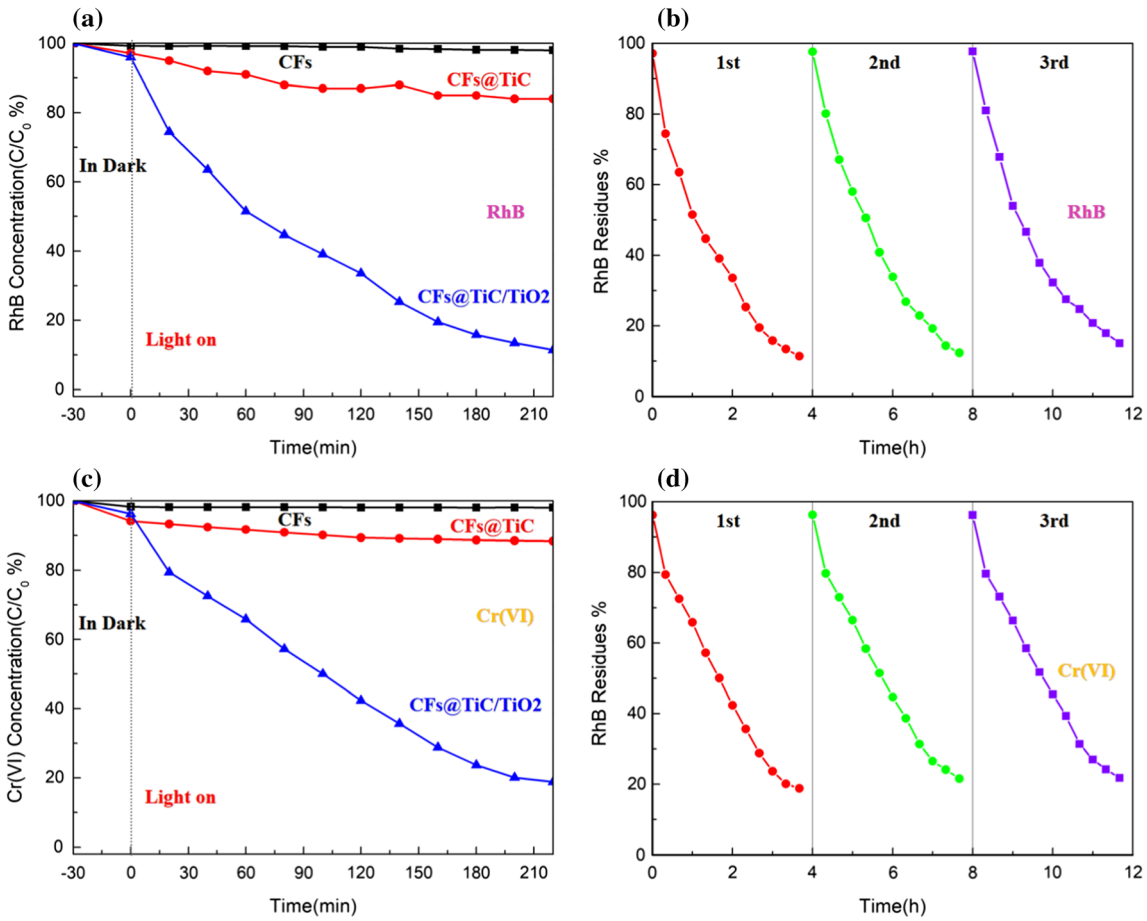

Figure 6 **a** Catalytic degradation of RhB, **b** repeating experiments of RhB with CFs@TiC/TiO_2, **c** catalytic reduction of Cr(VI), **d** repeating experiments of Cr(VI) with CFs@TiC/TiO_2.

By comparing the microstructure and XPS analysis of the CFs@TiC/TiO_2 before and after the reaction, shown in Figs. 7 and 8, it is not difficult to find that the microstructure of the material was well preserved without the obvious phenomenon of membrane fracture and peeling. At the same time, XPS analysis showed no significant changes in the element chemical states on the composite surface. These are important properties for the stability of catalytic performance after repeating tests.

Fundamentals and characteristics of catalysts

The main reaction processes can be described by the following chemical reactions:

$$TiH_2 == Ti + H_2 \quad (1)$$

$$C + Ti == TiC \quad (2)$$

$$6TiC + 14NaOH + 17H_2O = = Na_2Ti_6O_{13} + 6Na_2CO_3 + 24H_2 \quad (3)$$

$$Na_2Ti_6O_{13} + 2HCl == H_2Ti_6O_{13} + 2NaCl \quad (4)$$

$$H_2Ti_6O_{13} == 3TiO_2 + H_2O \quad (5)$$

$$O_2 + e^- \rightarrow \cdot O_2^- \quad (6)$$

$$\cdot O_2^- + 2H^+ + e^- + hv \rightarrow 2 \cdot OH \quad (7)$$

$$\cdot O_2^- + h^+ + \cdot OH + RhB \rightarrow \text{degradation products} \quad (8)$$

$$Cr(VI) + 3e^- \rightarrow Cr(III) \quad (9)$$

The photocatalytic degradation mechanism is proposed in Fig. 9 c. The ability of the composite to absorb and utilize the visible light comes down to the fact that the carbon dopant acts as a sensitizer into the TiO_2 lattice of the prepared core–shell nanostructured material [37]. The existence of a Ti–O–C bond was

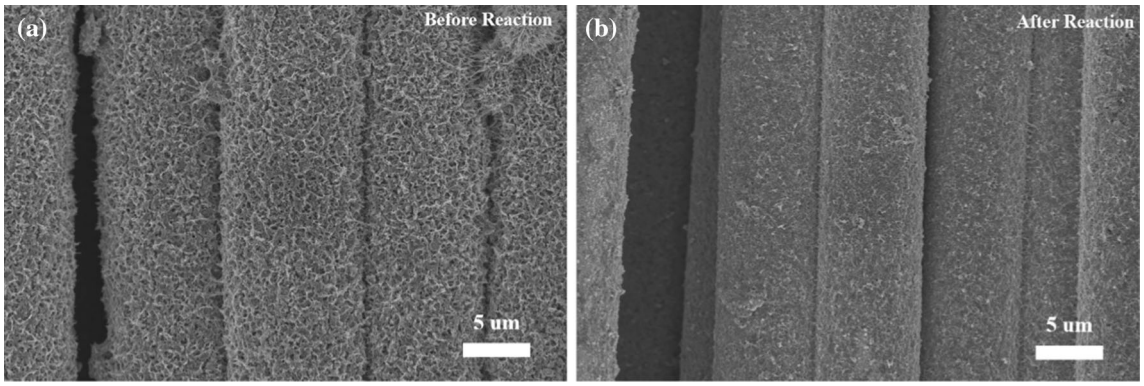

Figure 7 SEM of CFs@TiC/TiO_2 **a** before reaction and **b** after reaction.

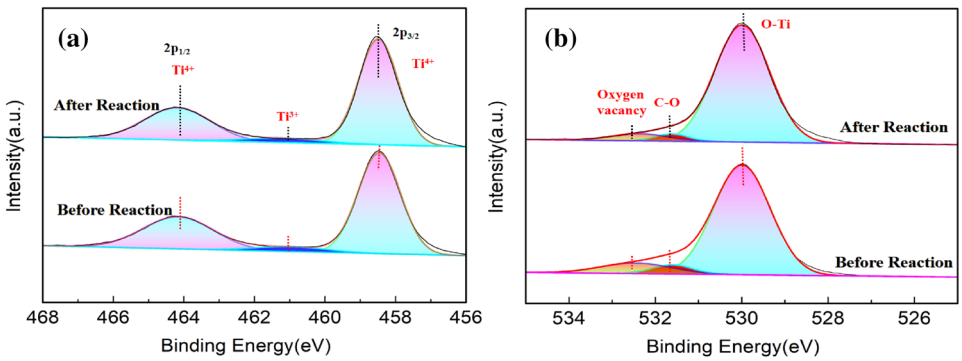

Figure 8 XPS analysis high-resolution scan of **a** Ti 2*p*(a) and **b** O 1s of CFs@TiC/TiO_2 before and after catalytic reaction.

confirmed by X-ray photoelectron spectroscopy. The residual TiC phase can be used as an electron emitter because of its high conductivity. The doping of carbon atoms introduces dopant states within the bandgap, which allows titanium dioxide to be excited by visible light. With the help of the Fermi level of titanium carbide, the fast electron transfer can be achieved, which improves the separation of the excited holes and electrons in the TiO_2. When the CFs@TiC/TiO_2 photocatalyst was irradiated with the visible light, the electrons were excited to the conduction band of the TiO_2. They can travel rapidly to the TiC and are subsequently captured by O_2 in the solution. At the same time, the holes in the VB react with H_2O/OH^- to create oxidative radicals. Anatase TiO_2 reacts with O_2 and H_2O to produce superoxide radical and ·OH under the visible light [40]. As shown in Fig. 9a and b, the reactive species required for the redox reaction were confirmed by ESR test results. These active radicals were directly involved in the catalytic oxidation of RhB and the reduction of Cr(VI).

Conclusions

In this work, the CFs@TiC precursor was prepared with CFs as the substrate. TiC/TiO_2 heterostructure was grown on the surface of CFs by hydrothermal, proton exchange, and calcination method. By simply controlling the reaction time, the reaction process can be controlled and samples with different micro-nanostructures can be obtained with shapes including needles, flowers, and networking morphology. The nanostructured materials provide a large surface area with a large number of reactive sites for catalysis, which results in good catalytic activities for both the degradation of RhB and the reduction of Cr(VI) under visible light excitation. Repeated experiments demonstrate the good stability of the photocatalytic activity. The catalytic mechanism and reaction processes are also discussed. The proposed simple and easy-to-control preparation technology has broad application prospects in the fields of water treatment and active liquid filtration. It provides new ideas for the application of CFs.

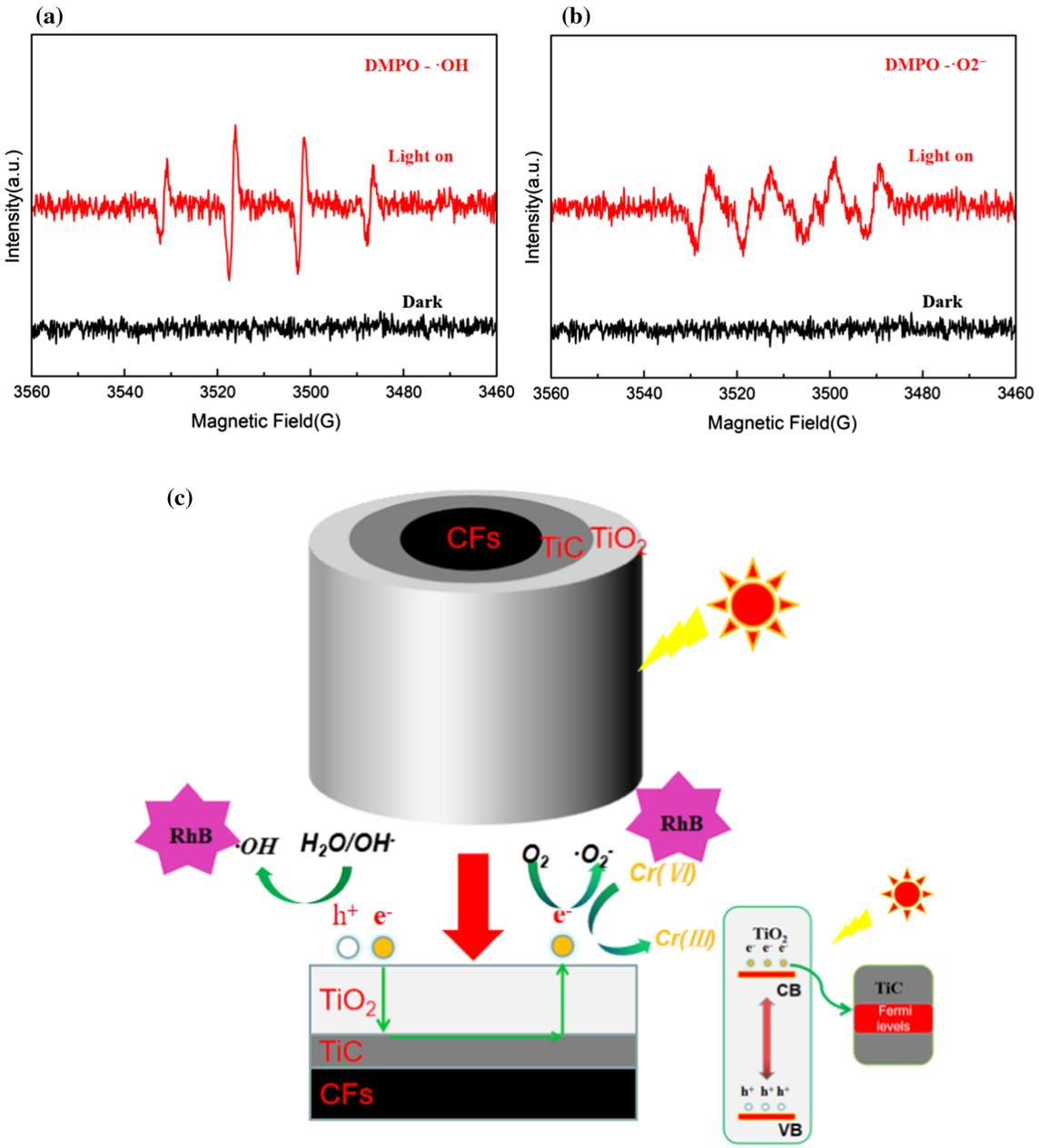

Figure 9 **a** ESR spectra for·OH, **b** ESR spectra for·O_2^-, **c** schematic diagram of catalytic mechanism.

Acknowledgements

The authors grateful for the financial support provided by National Project (No.41422XXX) and Natural Science Foundation for Young Scientists of Hunan Province (Grant No. 2019JJ50815). The author wishes to thank the teachers of the state key laboratory of powder metallurgy of Central South University for their help in sample testing.

Compliance with ethical standards

Conflict of interest We declare that we have no financial and personal relationships with other people or organizations that can inappropriately influence our work. There is no professional or other personal interest of any nature or kind in any product, service and company that could be construed as influencing the position presented in, or the review of, the manuscript entitled.

References

[1] Shi Z, Zhang Y, Shen X, Duoerkun G, Zhu B, Zhang L, Li M, Chen Z (2020) Fabrication of g-C_3N_4/BiOBr heterojunctions on carbon fibers as weaveable photocatalyst for degrading tetracycline hydrochloride under visible light. Chem Eng J 386:124010

[2] Zhang Y, Luo L, Zhang L et al (2019) Synthesis of MoS_2/CdS heterostructures on carbon-fiber cloth as filter-membrane-shaped photocatalyst for purifying the flowing wastewater under visible-light illumination. ChemCatChem 11:2855–2863

[3] Kozlova EA, Parmon VN (2017) Heterogeneous semiconductor photocatalysts for hydrogen production from aqueous solutions of electron donors. Russ Chem Rev 86:870–906

[4] Low JX, Yu JG, Jaroniec M, Wageh S, Al-Ghamdi AA (2017) Heterojunction photocatalysts. Adv Mater 29:1601694

[5] Christoforidis KC, Fornasiero P (2017) Photocatalytic hydrogen production: a rift into the future energy supply. ChemCatChem 9:1523–1544

[6] Guayaquil-Sosa JF, Serrano-Rosales B, Valadés-Pelayo PJ, de Lasa H (2017) Photocatalytic hydrogen production using mesoporous TiO_2 doped with Pt. Appl Catal B Environ 211:337–348

[7] Jia Y, Zhan S, Ma S, Zhou Q (2016) Fabrication of TiO_2–Bi_2WO_6 binanosheet for enhanced solar photocatalytic disinfection of *E. coli*: insights on the mechanism. ACS Appl Mater Interfaces 8:6841–6851

[8] Yun HJ, Lee H, Joo JB, Kim ND, Kang MY, Yi J (2010) Facile preparation of high performance visible light sensitive photo-catalysts. Appl Catal B Environ 94:241–247

[9] Gaya UI, Abdullah AH (2008) Heterogeneous photocatalytic degradation of organic contaminants over titanium dioxide: a review of fundamentals, progress and problems. J Photochem Photobiol C 9:1–12

[10] Zhang J, Xiao X, Nan J (2010) Hydrothermal-hydrolysis synthesis and photocatalytic properties of nano-TiO_2 with an adjustable crystalline structure. J Hazard Mater 176:617–622

[11] Herrmann JM (1999) Heterogeneous photocatalysis: fundamentals and applications to the removal of various types of aqueous pollutants. Catal Today 53:115–129

[12] Sharotri N, Sharma D, Sud D (2019) Experimental and theoretical investigations of Mn–N-co-doped TiO_2 photocatalyst for visible light induced degradation of organic pollutants. J Mater Res Technol 8:3995–4009

[13] Chen HJ, Yang YL et al (2019) Separable and recyclable meso-carbon@TiO_2/carbon fiber composites for visible-light photocatalysis and photoelectrocatalysis. Sustain Mater Technol 21:e00105

[14] Kibombo HS, Peng R, Rasalingam S, Koodali RT (2012) Versatility of heterogeneous photocatalysis: synthetic methodologies epitomizing the role of silica support in TiO_2 based mixed oxides. Catal Sci Technol 2:1737–1766

[15] Li A, Jin Y, Muggli D et al (2013) Nanoscale effects of silica particle supports on the formation and properties of TiO_2 nanocatalysts. Nanoscale 5:5854–5862

[16] Bellardita M, Addamo M, Di Paola A, Marci G, Palmisano L, Cassar L, Borsa M (2010) Photocatalytic activity of TiO_2/SiO_2 systems. J Hazard Mater 174:707–713

[17] Chen YH, Hsieh DC, Shang NC (2011) Efficient mineralization of dimethyl phthalate by catalytic ozonation using TiO_2/Al_2O_3 catalyst. J Hazard Mater 192:1017–1025

[18] Anderson C, Bard AJ (1997) Improved photocatalytic activity and characterization of mixed TiO_2/SiO_2 and TiO_2/Al_2O_3 materials. J Phys Chem B 101:2611–2616

[19] Sivapatarnkun J, Hathaisamit K, Pudwat S (2017) High photocatalytic activity of F-TiO_2 on activated carbon. Mater Today Proc 4:6495–6501

[20] Ali S, Li Z, Chen S et al (2019) Synthesis of activated carbon-supported TiO_2-based nano-photocatalysts with well recycling for efficiently degrading high-concentration pollutants. Catal Today 335:557–564

[21] Guo WX, Zhang F, Lin CJ, Wang ZL (2012) Direct growth of TiO_2 nanosheet arrays on carbon fibers for highly efficient photocatalytic degradation of methyl orange. Adv Mater 24:4761–4764

[22] Li M, Lu B, Ke QF, Guo YJ, Guo YP (2017) Synergetic effect between adsorption and photodegradation on nanostructured TiO_2/activated carbon fiber felt porous composites for toluene removal. J Hazard Mater 333:88–98

[23] Saito N, Aoki K, Usui Y et al (2011) Application of carbon fibers to biomaterials: a new era of nano-level control of carbon fibers after 30-years of development. Chem Soc Rev 40:3824–3834

[24] Gu X, Yu N, Zhang L, Yang J, Hu J, Chen Z (2015) Growth of TiO_2 nanorod bundles on carbon fibers as flexible and weaveable photocatalyst/photoelectrode. RSC Adv 5:102868–102876

[25] Shen X, Zhang T, Xu P, Zhang L, Liu J, Chen Z (2017) Growth of C_3N_4 nanosheets on carbon-fiber cloth as flexible and macroscale filter-membrane-shaped photocatalyst for degrading the flowing wastewater. Appl Catal B Environ 219:425–431

[26] Yuan R, Zheng J, Guan R, Zhao Y (2005) Surface characteristics and photocatalytic activity of TiO_2 loaded on activated carbon fibers. Colloids Surf A 254:131–136

[27] Liu JH, Yang R, Li SM (2006) Preparation and application of efficient TiO_2/ACFs photocatalyst. J Environ Sci 18:979–982

[28] Guo T, Bai Z, Wu C, Zhu T (2008) Influence of relative humidity on the photocatalytic oxidation (PCO) of toluene by TiO_2 loaded on activated carbon fibers: PCO rate and intermediates accumulation. Appl Catal B Environ 79:171–178

[29] Zhao W, Bai Z, Ren A, Guo B, Wu C (2010) Sunlight photocatalytic activity of CdS modified TiO_2 loaded on activated carbon fibers. Appl Surf Sci 256:3493–3498

[30] Shen X, Song L, Luo L et al (2018) Preparation of TiO_2/C_3N_4 heterojunctions on carbon-fiber cloth as efficient filter-membrane-shaped photocatalyst for removing various pollutants from the flowing wastewater. J Colloid Interface Sci 532:798–807

[31] Ma L, Li N, Wu G et al (2018) Interfacial enhancement of carbon fiber composites by growing TiO_2 nanowires onto amine-based functionalized carbon fiber surface in supercritical water. Appl Surf Sci 433:560–567

[32] Wang Y, Deng H, Ye C, Hu K, Yan K (2019) Facile synthesis of mesoporous TiC-C nanocomposite microsphere efficient for hydrogen evolution. J Alloys Compd 775:348–352

[33] Chen WF, Schneider JM, Sasaki K et al (2014) Tungsten carbide-nitride on graphene nanoplatelets as a durable hydrogen evolution electrocatalyst. Chemsuschem 7:2414–2418

[34] Ferri T, Gozzi D, Latini A (2007) Hydrogen evolution reaction (HER) at thin film and bulk TiC electrodes. Int J Hydrog Energy 32:4692–4701

[35] Calderon NR, Martínez-Escandell M, Narciso J, Rodríguez-Reinoso F (2009) The combined effect of porosity and reactivity of the carbon preforms on the properties of SiC produced by reactive infiltration with liquid Si. Carbon 47:2200–2210

[36] Zhang Y, Shi Z, Luo L et al (2020) Construction of titanium dioxide/cadmium sulfide heterojunction on carbon fibers as weavable photocatalyst for eliminating various contaminants. J Colloid Interface Sci 561:307–317

[37] Yang C, Zhang X, Qin J, Shen X, Yu R, Ma M, Liu R (2017) Porous carbon-doped TiO_2 on TiC nanostructures for enhanced photocatalytic hydrogen production under visible light. J Catal 347:36–44

[38] Nakata K, Ochiai T, Murakami T, Fujishima A (2012) Photoenergy conversion with TiO_2 photocatalysis: new materials and recent applications. Electrochim Acta 84:103–111

[39] Nakata K, Fujishima A (2012) TiO_2 photocatalysis: design and applications. J Photochem Photobiol C 13:169–189

[40] Shen X, Zhang Y, Duoerkun G, Shi Z, Liu J, Chen Z, Keung Wong P, Zhang L (2019) Vis-NIR light-responsive photocatalytic activity of C_3N_4–Ag–Ag_2O heterojunction-decorated carbon-fiber cloth as efficient filter-membrane-shaped photocatalyst. ChemCatChem 11:1362–1373